COMPUTATIONAL ANALYSIS OF VISCOUS DISSIPATION AND JOULE-HEATING EFFECTS ON NON-DARCY MHD NATURAL CONVECTION FLOW FROM A HORIZONTAL CYLINDER IN POROUS MEDIA WITH INTERNAL HEAT GENERATION

V.Ramachandra Prasad   **A.Subba Rao**   **O.Anwar Bég**

Computational analysis of viscous dissipation and Joule-heating effects on non-Darcy MHD natural convection flow from a horizontal cylinder in porous media with internal heat generation

V.Ramachandra Prasad[*]   A.Subba Rao[†]   O.Anwar Bég,[‡]

Abstract

In the present paper we examine the effects of viscous dissipation, Joule heating and heat source/sink on non-Darcy MHD natural convection heat transfer flow over permeable horizontal circular cylinder in a porous medium. The boundary layer equations, which are parabolic in nature, are normalized into non-similar form and then solved numerically with the well-tested, efficient, implicit, stable Keller-box finite difference scheme. A parametric study illustrating the influence of Darcy parameter (Da), Forchheimer parameter (Λ) , Grashof number(Gr), heat source/sink parameter (Ω) and viscous dissipation parameter (Ec) on the fluid velocity, temperature as well as local skin-friction and Nusselt numbers is conducted Increasing Forchheimer inertial drag parameter (Λ) retards the flow considerably but enhances temperatures. Increasing viscous dissipation parameter(Ec) is found to elevate velocities i.e. accelerate the flow and increase temperatures. Increasing heat source/sink parameter (Ω) is found to elevate velocities and increase temperatures. Increasing the Grashof number (Gr) is found to elevate the velocity and decrease the temperatures. Local skin friction number is found to be increases with increasing heat source/sink parameter (Ω) where as Local Nusselt number is found to decrease with increasing heat source/sink parameter (Ω).

Keywords: Viscous dissipation, Joule heating, Keller-box numerical method, Heat transfer, Skin friction, Nusselt number.

[*]Department of Mathematics, Madanapalle Institute of Technology and Science, Madanapalle-517325, India, e-mail: rcpmaths@gmail.com

[†]Department of Mathematics, Sri Venkateswara University, Tirupathi-517502, Andrapradesh, India, e-mail: subbumaths@yahoo.com

[‡]Gort Engovation(Propulsion and Biomechanics), Southmere Avenue., Bradford, BD7 3NU, England, UK, email: gortoab@gmail.com

37

Nomenclature

a	radius of the cylinder	Nu	Local Nusselt number
B_0	the externally imposed radial magnetic field	Pr	Prandtl number
C_f	skin friction coefficient	q_r	radiative heat flux
Da	Darcy parameter	Sc	Schmidt number
f	non-dimensional steam function	Sh	local Sherwood number
g	acceleration due to gravity	T	temperature
Gr	Grashof number	u, v	non-dimensional velocity components along the x- and y- directions, respectively
K	thermal diffusivity		
$k*$	the mean absorption coefficient	x, y	non-dimensional Cartesian coordinates along the surface of the cylinder and normal to it,respectively
M	the magnetic parameter		
N	buoyancy ratio parameter		

Greek symbols

α	thermal diffusivity	ν	kinematic viscosity
β, β^*	the coefficients of thermal expansion and concentration expansion, respectively	θ	non-dimensional temperature
Φ	the azimuthal coordinate	ρ	density
φ	non-dimensional concentration	σ	the electrical conductivity
Γ	the Forchheimer inertial drag coefficient	$\sigma*$	the Stefan-Boltzmann constant
η	the dimensionless radial coordinate	ξ	the dimensionless tangential coordinate
μ	dynamic viscosity	ψ	dimensionless stream function

Subscripts

w	conditions on the wall	∞	free stream conditions

1   Introduction

Transport processes in porous media can involve fluid, heat transfer in single or multi-phase scenarios. Such flows with and without buoyancy effects arise frequently in many branches of chemical engineering and owing to their viscous-dominated nature are generally simulated using the Darcy model. Applications of such flows include chip-based microfluidic chromatographic separation devices Dorfmann and Brenner [1], heat transfer in radon saturating permeable regimes Minkin [2] flows in ceramic filter components of Integrated gasification combined

cycles (IGCC) Seo et al. [3] separation of Carbon Dioxide from the gas phase with aqueous absorbents (water and diethanolamine solution) in microporous hollow fibre membrane modules Al-saffar et al. [4] and monolithic adsorbent flows consisting of micro-porous zeolite particles embedded in a polyamide matrix Ledvinkova et al. [5]. Porous media flow simulations are also critical in convective processes in hygroscopic materials Turner et al. [6], electroremediation in soil decontamination technique wherein an electric field applied to a porous medium generates the migration of ionic species in solution Pomés et al. [7], reactive transport in tubular porous media reactors Islam, [8], perfusive bed flows Albusairi and Hsu [9], gelation of biopolymers in porous media which arise in petroleum recovery and in subsurface heavy metal stabilization Khachatoorian and Yen, [10]. Further still applications arise in the sorption and diffusion of volatile organic compounds (VOCs) in soils Arocha et al. [11], polymeric filtration in permeable barriers Zueco et al [12] and axial flow through chromatographic columns packed with non-rigid gels Östergren and Trägørdh [13]. Frequently working fluids may possess an *electrically-conducting* nature and will respond to *magnetic fields*. For example in the liquid-encapsulated Czochralski (LEC) process Dennis and Dulikravich [14] a single compound semiconductor crystal (e.g. indium phosphide or gallium antimonide) is grown via solidification of an initially molten semiconductor contained in a crucible. The motion of the electrically conducting molten semiconductor can be controlled with an externally applied magnetic field. Magneto hydrodynamic flows also arise in rheological wire coating processes Shafieenejad *et al.* [15], pulsed-field-gradient NMR analysis of permeable transport Holmes *et al.* [16], magnetic field control of polymer alignment in Carbon nanotubes Garmestani *et al.* [17] and MHD levitation control of diamagnetic material manufacture Mogi *et al.* [18]. In all these studies the strong and efficient effect of steady transverse magnetic fields has been identified. Bég *et al.* [19] used a network electro-thermodynamic computational method to analyze the transient MHD heat transfer in a porous medium parallel plate channel with electrodynamic effects. Bég *et al.* [20] also studied hydromagnetic free convection boundary layers from a sphere embedded in a porous medium. Transport from a cylinder embedded in porous media also has important applications in geothermics, environmental contamination Alves *et al.* [21] and chemical processing Mauguet *et al.* [22]. Magnetohydrodynamic convection in porous media is of considerable importance also in alternate energy systems modeling Azzam, [23]. El-Amin [24] has analyzed numerically magneto-convection from a horizontal cylinder in porous media.

In all the above studies, the effects of both viscous dissipation and Joule-heating are neglected. Gebhart [25] has shown that the viscous dissipation effect plays an important role in natural convection in various devices that are sub-

jected to large deceleration or that operate at high rotational speeds, in strong gravitational field processes on large scales (on large planets), and in geological processes. With this understanding, Takhar and Soundalgekar [26] studies the effects of viscous and Joule heating on the natural convection problem posed by Sparrow and Cess [27], using the series expansion method proposed by Gebhart [25]. Yih [28] has analyzed viscous and Joule heating effects on non-Darcy MHD natural convection flow over a permeable sphere in porous media with internal heat generation. Duwairi et al. [29] have studied viscous and Joule heating effects over an isothermal cone in saturated porous media.

In the present paper, we propose to study the effects of viscous dissipation, Joule heating and heat source/sink effects on the flow of an electrically conducting, viscous, incompressible heat flow past permeable horizontal circular cylinder in a non-Darcy porous medium. The governing equations, which describe the problem, were transformed and solved using Keller Box scheme. Such as study has, to the authors' knowledge not appeared hitherto in the literature.

2   Mathematical model

Consider the steady, laminar, two-dimensional, incompressible, electrically-conducting, buoyancy - driven convection heat transfer flow from a horizontal cylinder embedded in an isotropic, homogenous, fully-saturated porous medium. Figure 1 shows the flow model and physical coordinate system. The x-coordinate is measured along the circumference of the horizontal cylinder from the lowest point and the y-coordinate is measured normal to the surface, with a denoting the radius of the horizontal cylinder. $\Phi = x/a$ is the angle of the y-axis with respect to the vertical $(0 \leq \Phi \leq \pi)$. The gravitational acceleration, g, acts downwards. Magnetic Reynolds number is assumed to be small enough to neglect magnetic induction effects. Hall current and ionslip effects are also neglected since the magnetic field is weak. It is also assumed that the Boussineq approximation holds i.e. that density variation is only experienced in the buoyancy term in the momentum equation. Additionally the electron pressure (for weakly conducting fluids) and the thermoelectric pressure are negligible.

Both the horizontal cylinder and the fluid are maintained initially at the same temperature. Instantaneously they are raised to a temperature $T_w (> T_\infty)$ which remain unchanged thereafter. The effects of viscous dissipation, Joule heating and internal heat generation are included in this work. In line with the approach of Yih [28] and introducing the boundary layer approximations, the governing conservation equations can be written as follows:
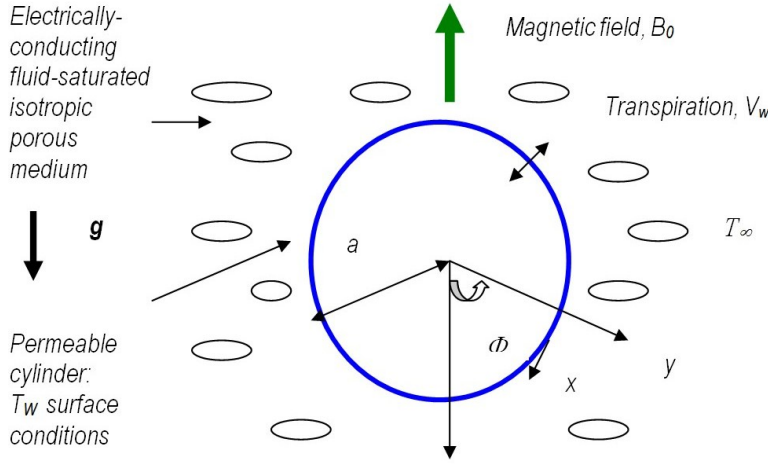
Figure 1: Physical Model and Coordinate System

$$u\frac{\partial u}{\partial x} + v\frac{\partial u}{\partial y} = g\beta(T - T_\infty)\sin\left(\frac{x}{a}\right) + \nu\frac{\partial^2 u}{\partial y^2} - \frac{\sigma\beta_0^2}{\rho}u - \frac{\nu}{K}u - \Gamma u^2 \qquad (1)$$

$$u\frac{\partial T}{\partial x} + v\frac{\partial T}{\partial y} = \alpha\frac{\partial^2 T}{\partial y^2} + \frac{\nu}{c_p}\left(\frac{\partial u}{\partial y}\right)^2 + \frac{\sigma B_0^2}{\rho c_p}u^2 + \frac{Q}{\rho c_p}(T - T_\infty) \qquad (2)$$

The boundary conditions are prescribed at the cylinder surface and the edge of the boundary layer regime, respectively as follows:

$$y = 0: \quad u = 0, \quad v = V_w, \; T = T_w \qquad (3)$$

$$y = \infty: \quad u = 0, \; T = T_\infty$$

where u and v denote the velocity components in the x - and y- directions respectively, K and Γ are the respective permeability and the inertia coefficient of the porous medium, ν is the kinematic viscosity of the conducting fluid, β is the coefficients of concentration expansion, respectively, T is the temperature respectively, σ is the electrical conductivity, B_0 is the externally imposed magnetic field in the y-direction, ρ is the density, c_p is the specific heat capacity, T_∞- is the volumetric rate of heat generation/absorption , α is the thermal diffusivity, T_∞ is the free stream temperature V_w is the uniform blowing/suction velocity. Implicit in the present model is the assumption that magnetic Reynolds number

is small and the induced magnetic field is negligible compared with the applied magnetic field. The Hall Effect is also neglected. It should be noted that in the momentum equation Eq.(2), the fifth term on the right hand side is the porous medium *Darcian drag force* representing pressure loss due to the presence of the porous medium. The sixth term on the same side is the *inertial drag force* (also referred to as the Forchheimer impedance) which accounts for additional pressure drop resulting from inter-pore-mixing appearing at high velocities, as described by Plumb and Huenefeld [30]. The stream function ψ is defined by $u = \partial\psi/\partial y$ and $v = -\partial\psi/\partial x$, therefore the continuity equation is automatically satisfied. Proceeding with the analysis we introduce the following dimensionless variables:

$$\xi = \frac{x}{a}, \qquad \eta = \frac{y}{a}\sqrt[4]{Gr}, \qquad f(\xi,\eta) = \frac{\psi}{\nu\xi\sqrt[4]{Gr}}$$

$$\theta(\xi,\eta) = \frac{T - T_\infty}{T_w - T_\infty}, \quad Gr = \frac{g\beta(T_w - T_\infty)a^3}{\nu^2} \tag{4}$$

Substituting Eq.(4) into Eqs.(1) to (3), we obtain the coupled, nonlinear, dimensionless partial differential equations for momentum, energy and species conservation for the regime:

$$f''' + ff'' - (1+\xi\Lambda)f'^2 + \frac{\sin\xi}{\xi}(\theta) - \left[M + \frac{1}{DaGr^{1/2}}\right]f' = \xi\left(f'\frac{\partial f'}{\partial\xi} - f''\frac{\partial f}{\partial\xi}\right) \tag{5}$$

$$\frac{\theta''}{\Pr} + f\theta' + \xi^2 Ec\left[f''^2 + Mf'^2\right] + \Omega\theta = \xi\left(f'\frac{\partial\theta}{\partial\xi} - \theta'\frac{\partial f}{\partial\xi}\right) \tag{6}$$

The transformed dimensionless boundary conditions are:

$$\eta = 0: \quad f' = 0, \quad f = f_w, \quad \theta = 1 \tag{7}$$

$$\eta \to \infty: \quad f' = 0, \quad \theta = 0$$

In the above equations, the primes denote the differentiation with respect to η, the dimensionless radial coordinate, ξ is the dimensionless tangential coordinate and Φ the azimuthal coordinate, $\Lambda = \Gamma a$ is the local inertia co-efficient (Forchheimer parameter), $M = \sigma B_0^2 a^2 / \rho\nu\sqrt{Gr}$ is the magnetic parameter, $Da = \frac{K}{a^2}$ is a Darcy parameter, $\Pr = \frac{\rho\nu c_p}{k}$ is the Prandtl number, $Ec = \frac{Gr\,\nu^2}{a^2 c_p(T_w - T_\infty)}$ is the Eckert number, $\Omega = \frac{Q\,a^2}{\rho c_p\nu Gr^{1/2}}$ is the heat source/sink parameter, $\Omega > 0$ for $Q > 0$ (the case of heat source), $\Omega < 0$ for $Q < 0$ (the case of heat sink), and Gr is the Grashof (free convection) parameter The engineering

design quantities of physical interest include the skin-friction coefficient, Nusselt number which are given by:

$$\frac{1}{2}C_f \sqrt[4]{Gr} = \xi f''(\xi, 0) \tag{8a}$$

$$\frac{Nu}{\sqrt[4]{Gr}} = -\theta'(\xi, 0) \tag{8b}$$

3 Numerical solution with implicit difference code

In this study the efficient Keller-Box implicit difference method has been employed to solve the general flow model defined by equations (5) to (6) with boundary conditions (7a) and (7b). This method, originally developed for low speed aerodynamic boundary layers by Keller [31] has been employed in a diverse range of nonlinear magneto hydrodynamics and coupled heat transfer problems. These include magnetic boundary layers Chiam [32], wavy thermal boundary layers Rees and Pop, [33], rotating hydro magnetic convection Hossain *et al.,* [34], radiative-convective porous media gas flows Bég *et al.* [38], thermal convection in porous regimes Rees and Hossain, [36], magneto-viscoelastic heat transfer in porous media Bég *et al.* [37], radiation-convection viscoelastic boundary layers Bég *et al.* [38], hydromagnetic convection from an elastic cylinder Ishak *et al.* [39] and hydro magnetic thermophoretic mixed convection in porous media Damseh *et al.* [40]. Very few of these papers however have provided guidance for researchers as to customization of the Keller-box scheme to magneto hydrodynamic heat transfer problems. We therefore present a more detailed exposition here. Essentially 4 phases are central to the Keller Box Scheme. These are:

a) Reduction of the Nth order partial differential equation system to N 1st order equations

b) Finite Difference Discretization

c) Quasilinearization of Non-Linear Keller Algebraic Equations

d) Block-tridiagonal Elimination of Linear Keller Algebraic Equations

A 2-Dimensional computational grid is imposed on the $\xi - \eta$ plane as sketched below. The stepping process is defined by:

$$\xi_o = 0; \xi_n = \xi_{n-1} + k_n, n = 1, 2, \ldots N \tag{14a}$$

$$\eta_0 = 0; \eta_j = \eta_{j-1} + h_j, j = 1, 2 \ldots J \tag{14b}$$

where k_n and h_j denote the step distances in the ξ and η directions respectively. Denoting Σ as the value of any variable at station ξ_n, η_j, and the following *central* difference approximations are substituted for each reduced variable and their *first order* derivatives, viz:

$$(\Sigma)_{j-1/2} = [\Sigma^n{}_j + \Sigma^n_{j-1} + \Sigma^{n-1}{}_j + \Sigma^{n-1}_{j-1}]/4 \tag{15a}$$

$$(\partial\Sigma/\partial\xi)^{n-1/2}{}_{j-1/2} = [\Sigma^n{}_j + \Sigma^n_{j-1} - \Sigma^{n-1}{}_j - \Sigma^{n-1}_{j-1}]/4k_n \tag{15b}$$

$$(\partial\Sigma/\partial\eta)^{n-1/2}{}_{j-1/2} = [\Sigma^n{}_j + \Sigma^n_{j-1} - \Sigma^{n-1}{}_j - \Sigma^{n-1}_{j-1}]/4h_j \tag{15c}$$

where k_n = streamwise stepping distance (ξ-mesh spacing) and h_j = spanwise stepping distance (η-mesh spacing) defined as follows:

$$\eta_{j-1/2} = [\eta_j + \eta_{j-1}]/2 \tag{16a}$$

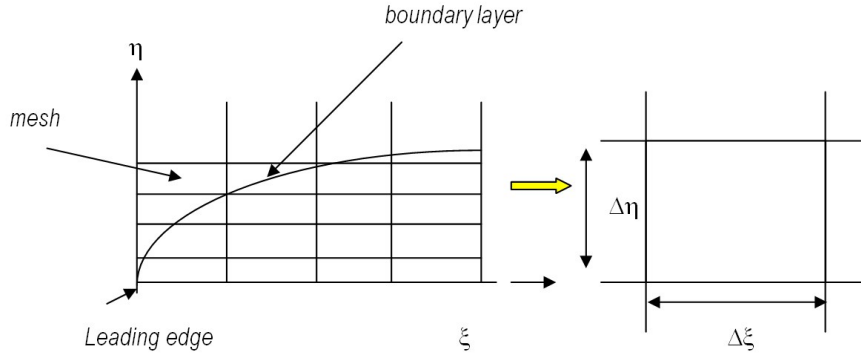$$\xi^{n-1/2} = [\xi^n + \xi^{n-1}]/2 \tag{16b}$$

Figure 2: Grid meshing and a "Keller Box" computational cell

Phase a) Reduction of the Nth order partial differential equation system to N 1st order equations

Equations (5) to (6) subject to the boundary conditions (7) are first written as a system of first-order equations. For this purpose, we introduce new dependent variables $u(x, y)$, $v(x, y)$, $t(x, y)$, and $s(x, y)$ as the variables for temperature, velocity respectively. Therefore, we obtain the following five first-order equations:

$$f' = u \tag{17a}$$

$$u' = v \tag{17b}$$

$$s' = t \tag{17c}$$

$$v' + fv - (1 + \xi\Lambda)u^2 + \frac{\sin\xi}{\xi}[s] - \left[M + \frac{1}{DaGr^{1/2}}\right]u = \xi\left(u\frac{\partial u}{\partial\xi} - v\frac{\partial f}{\partial\xi}\right) \tag{17d}$$

$$\frac{t'}{\text{Pr}} + ft + \xi^2 Ec\left[v^2 + Mu^2\right] + \Omega s = \xi\left(u\frac{\partial s}{\partial\xi} - t\frac{\partial f}{\partial\xi}\right) \tag{17e}$$

where primes denote differentiation with respect to η. In terms of the dependent variables, the boundary conditions become:

$$\begin{array}{llll} \eta = 0: & u = 0, & f = f_w, & s = 1 \\ \eta = \infty: & u = 0, & s = 0 & \end{array} \tag{18}$$

Phase b) Finite Difference Discretization

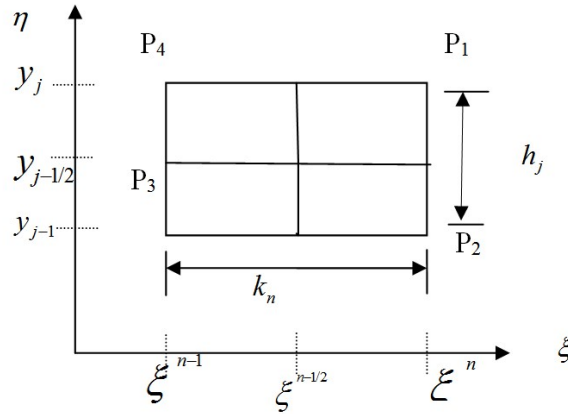The net rectangle considered in the $x - y$ plane is shown in figure 3, and the net points are denoted by:

Figure 3: Net "Keller Box" for difference approximations

$$\xi^0 = 0, \qquad \xi^n = \xi^{n-1} + k_n, \qquad n = 1, 2, ...N \tag{19a}$$

$$\eta_0 = 0, \qquad \eta_j = \eta_{j-1} + h_j, \qquad j = 1, 2, ...J, \qquad \eta_J \equiv \eta_\infty, \tag{19b}$$

where k_n is the $\Delta\xi-$ spacing and h_j is the $\Delta\eta-$spacing. Here n and j are just sequence numbers that indicate the coordinate location. We approximate the

quantities (f, u, v, s, t) at points (ξ^n, η_j) of the net by (f_j^n, u_j^n, v_j^n, s_j^n, t_j^n), which we denote as *net functions*. We also employ the notion $(\ )_j^n$ for points and quantities midway between net points and for any net function:

$$\xi^{n-1/2} \equiv \frac{1}{2}\left(\xi^n + \xi^{n-1}\right), \qquad \eta_{j-1/2} \equiv \frac{1}{2}\left(\eta_j + \eta_{j-1}\right) \qquad (20\text{a,b})$$

$$()_j^{n-1/2} = \frac{1}{2}\left[()_j^n + ()_j^{n-1}\right] \quad and \quad ()_{j-1/2}^n = \frac{1}{2}\left[()_j^n + ()_{j-1}^n\right] \qquad (20\text{c,d})$$

The derivatives in the x-direction are replaced by finite difference approximations. For any net function ( ), generally we have:

$$\frac{\partial\,()}{\partial x} = \frac{()^n - ()^{n-1}}{k_n}. \qquad (20\text{e})$$

$$y_j k_n \xi^n \xi^{n-1/2} \xi^{n-1}\, y_{j-1} y_{j-1/2} y_j \eta \xi$$

We write the difference equations that are to approximate equations 17(a) – 17(e) by considering one mesh rectangle as shown in Figure 1. We start by writing the finite-difference approximations of the *ordinary differential equations* 17(a) to 17(c) for the midpoint ($\xi^n, \eta_{j-1/2}$) of the segment P_1P_2, using *centered-difference* derivatives. This process is called "centering about ($\xi^n, \eta_{j-1/2}$)". This gives:

$$\frac{\left(f_j^n - f_{j-1}^n\right)}{h_j} = \frac{1}{2}\left(u_j^n + u_{j-1}^n\right) = u_{j-1/2}^n, \qquad (21\text{a})$$

$$\frac{\left(u_j^n - u_{j-1}^n\right)}{h_j} = \frac{1}{2}\left(v_j^n + v_{j-1}^n\right) = v_{j-1/2}^n, \qquad (21\text{b})$$

$$\frac{\left(s_j^n - s_{j-1}^n\right)}{h_j} = \frac{1}{2}\left(t_j^n + t_{j-1}^n\right) = t_{j-1/2}^n, \qquad (21\text{c})$$

The finite-difference forms of the *partial differential equations* (17 d) to (17 e) are approximated by centering about the midpoint $\left(\xi^{n-1/2}, \eta_{j-1/2}\right)$ of the rectangle $P_1P_2P_3P_4$. This can be done in two steps. In the first step, we center equations (17d) to (17e) about the point $\left(\xi^{n-1/2}, \eta\right)$ without specifying y. The differenced version of equations (17 d) to (17 e) at $\xi^{n-1/2}$ then take the form:

$$(v')^n + (1+\alpha)\,(fv)^n - (1+\alpha+\xi\Lambda)\,\left(u^2\right)^n - \left(M + \frac{1}{DaGr^{1/2}}\right)u^n +$$
$$\alpha v^{n-1} f^n - \alpha f^{n-1} v^n + B\left(s^n\right) = \left[-\left(v'\right) + (\alpha-1)\,(fv) + \right. \qquad (22\text{a})$$
$$\left. (1-\alpha+\xi\Lambda)\,\left(u^2\right) - B\,(s) + \left(M + \frac{1}{DaGr^{1/2}}\right)u\right]^{n-1}$$

$$\frac{1}{\Pr}\left(t'\right)^n + \left(1+\alpha\right)\left(ft\right)^n + \xi^2 Ec\left[\left(v^n\right)^2 + M\left(u^n\right)^2\right] +$$
$$\Omega s^n - \alpha\left(us\right)^n + \alpha s^{n-1}u^n - \alpha u^{n-1}s^n - \alpha f^{n-1}t^n + \alpha t^{n-1}f^n =$$
$$\left[-\frac{1}{\Pr}\left(t'\right) + \left(\alpha-1\right)\left(ft\right) - \xi^2 Ec\left[\left(v\right)^2 + M\left(u\right)^2\right] - \Omega s - \alpha\left(us\right)\right]^{n-1} \tag{22b}$$

Where we have used the abbreviations

$$\alpha = \frac{\xi^{n-1/2}}{k_n} \tag{23a}$$

$$B = \frac{\sin\left(\xi^{n-1/2}\right)}{\xi^{n-1/2}} \tag{23b}$$

and where the notation $[]^{n-1}$ corresponds to quantities in the square bracket evaluated at $\xi = \xi^{n-1}$. Next, we center equations (22 a-b) about the point $\left(\xi^{n-1/2}, \eta_{j-1/2}\right)$ by using equation (20d) yielding:

$$\left(\frac{v_j^n - v_{j-1}^n}{h_j}\right) + \left(1+\alpha\right)\left(f_{j-1/2}^n v_{j-1/2}^n\right) - \left(1+\alpha+\xi\Lambda\right)\left(u_{j-1/2}^n\right)^2 -$$

$$\left(M + \frac{1}{DaGr^{1/2}}\right)u_{j-1/2}^n + \alpha v_{j-1/2}^{n-1}f_{j-1/2}^n - \alpha f_{j-1/2}^{n-1}v_{j-1/2}^n + B\left(s_{j-1/2}^n\right) =$$

$$-\left[\left(\frac{v_j^{n-1} - v_{j-1}^{n-1}}{h_j}\right) + \left(1-\alpha\right)\left(f_{j-1/2}^{n-1}v_{j-1/2}^{n-1}\right)\right.$$

$$\left. + \left(\alpha-1-\xi\Lambda\right)\left(u_{j-1/2}^{n-1}\right)^2 + B\left(s_{j-1/2}^{n-1}\right) - \left(M + \frac{1}{DaGr^{1/2}}\right)u_{j-1/2}^{n-1}\right] \tag{24a}$$

$$\frac{1}{\Pr}\left(\frac{t_j^n - t_{j-1}^n}{h_j}\right) + \left(1+\alpha\right)\left(f_{j-1/2}^n t_{j-1/2}^n\right) + \xi^2 Ec\left[\left(v_{j-1/2}^n\right)^2 + M\left(u_{j-1/2}^n\right)^2\right] +$$

$$\Omega s_{j-1/2}^n - \alpha\left(u_{j-1/2}^n s_{j-1/2}^n\right) + \alpha s_{j-1/2}^{n-1}u_{j-1/2}^n - \alpha u_{j-1/2}^{n-1}s_{j-1/2}^n - \alpha f_{j-1/2}^{n-1}t_{j-1/2}^n +$$

$$\alpha t_{j-1/2}^{n-1}f_{j-1/2}^n = -\left[\frac{1}{\Pr}\left(\frac{t_j^{n-1} - t_{j-1}^{n-1}}{h_j}\right) + \left(1-\alpha\right)\left(f_{j-1/2}^{n-1}t_{j-1/2}^{n-1}\right) +\right.$$

$$\left.\xi^2 Ec\left[\left(v_{j-1/2}^{n-1}\right)^2 + M\left(u_{j-1/2}^{n-1}\right)^2\right] + \Omega s_{j-1/2}^{n-1} + \alpha\left(u_{j-1/2}^{n-1}s_{j-1/2}^{n-1}\right)\right] \tag{24b}$$

Equations (21) and (22) are imposed for $j= 1, 2\ldots J$ at given n, and the transformed boundary layer thickness,y_J is to be sufficiently large so that it is beyond the edge of the boundary layer.

At $\xi = \xi^n$, the boundary conditions (11) become

$$f_0^n = u_0^n = 0, \quad s_0^n = 1, \quad u_J^n = 0, \quad s_J^n = 0 \tag{25}$$

Phase c) Quasilinearization of Non-Linear Keller Algebraic Equations

Newton's Method is then employed to quasilinearize the equations (24 a-b). If we assume f_j^{n-1}, u_j^{n-1}, v_j^{n-1}, s_j^{n-1}, t_j^{n-1} to be know for $0 \leq j \leq J$, then equations (21), (24) and (25) are a system of equations for the solution of the unknowns $(f_j^n, u_j^n, v_j^n, s_j^n, t_j^n)$, $j = 0, 1, 2,\ldots..J$. For simplicity of notation we shall write the unknowns at $\xi = \xi^n$ as:

$$(f_j^n, u_j^n, v_j^n, s_j^n, t_j^n) \equiv (f_j, u_j, v_j, s_j, t_j). \tag{26}$$

Then the system of equations (21) and (24) can be written as (after multiplying with h_j)

$$f_j - f_{j-1} - \frac{h_j}{2} (u_j + u_{j-1}) = 0, \tag{27a}$$

$$u_j - u_{j-1} - \frac{h_j}{2} (v_j + v_{j-1}) = 0, \tag{27b}$$

$$s_j - s_{j-1} - \frac{h_j}{2} (t_j + t_{j-1}) = 0, \tag{27c}$$

$$(v_j - v_{j-1}) + \frac{(1+\alpha)\,h_j}{4} \left[(f_j + f_{j-1})(v_j + v_{j-1})\right] - \frac{h_j}{4}(1 + \alpha + \xi\Lambda) \times$$

$$(u_j + u_{j-1})^2 - \frac{h_j}{2}\left(M + \frac{1}{DaGr^{1/2}}\right)(u_j + u_{j-1}) + \frac{\alpha h_j}{2} v_{j-1/2}^{n-1}(f_j + f_{j-1}) -$$

$$\frac{\alpha h_j}{2} f_{j-1/2}^{n-1}(v_j + v_{j-1}) + \frac{Bh_j}{2}[s_j + s_{j-1}] = [R_1]_{j-1/2}^{n-1}$$

$$\tag{27d}$$

$$\frac{1}{\text{Pr}}\left(t_j - t_{j-1}\right) + \frac{(1+\alpha)h_j}{4}\left[(f_j + f_{j-1})(t_j + t_{j-1})\right] + \xi^2 Ec\frac{h_j}{4}\times$$

$$\left[(v_j + v_{j-1})^2 + M(u_j + u_{j-1})^2\right] + \Omega\frac{h_j}{2}(s_j + s_{j-1}) - \frac{\alpha h_j}{4}\times$$

$$[(u_j + u_{j-1})(s_j + s_{j-1})] + \frac{\alpha h_j}{2}s_{j-1/2}^{n-1}(u_j + u_{j-1}) - \frac{\alpha h_j}{2}u_{j-1/2}^{n-1}(s_j + s_{j-1}) -$$

$$\frac{\alpha h_j}{2}f_{j-1/2}^{n-1}(t_j + t_{j-1}) + \frac{\alpha h_j}{2}t_{j-1/2}^{n-1}(f_j + f_{j-1}) = [R_2]_{j-1/2}^{n-1}$$

$$(27e)$$

Where

$$[R_1]_{j-1/2}^{n-1} = -h_j\left[\left(\frac{v_j - v_{j-1}}{h_j}\right) + (1-\alpha)\left(f_{j-1/2}v_{j-1/2}\right) + \right.$$

$$(28a)$$

$$\left.(\alpha - 1 - \xi\Lambda)\left(u_{j-1/2}\right)^2 + B\left(s_{j-1/2}\right) - \left[M + \frac{1}{DaGr^{1/2}}\right]u_{j-1/2}\right]$$

$$[R_2]_{j-1/2}^{n-1} = -h_j\left[\frac{1}{\text{Pr}}\left(\frac{t_j - t_{j-1}}{h_j}\right) + (1-\alpha)\left(f_{j-1/2}t_{j-1/2}\right) + \right.$$

$$(28b)$$

$$\left.\xi^2 Ec\left[\left(v_{j-1/2}\right)^2 + M\left(u_{j-1/2}\right)^2\right] + \Omega s_{j-1/2} + \alpha\left(u_{j-1/2}s_{j-1/2}\right)\right]$$

$[R_1]_{j-1/2}^{n-1}$ and $[R_2]_{j-1/2}^{n-1}$ involve only know quantities if we assume that solution is known on $\xi = \xi^{n-1}$. To linearize the non-linear system of equations (27) using Newton's method, we introduce the following iterates:

$$f_j^{(i+1)} = f_j^{(i)} + \delta f_j^{(i)}, \qquad u_j^{(i+1)} = u_j^{(i)} + \delta u_j^{(i)}, \qquad v_j^{(i+1)} = v_j^{(i)} + \delta v_j^{(i)},$$

$$s_j^{(i+1)} = s_j^{(i)} + \delta s_j^{(i)}, \qquad t_j^{(i+1)} = t_j^{(i)} + \delta t_j^{(i)}.$$

$$(29)$$

Then we substitute these expressions into equations (27a) – (27e) except for the term ξ^{n-1}, and this yields:

$$\left(f_j^{(i)} + \delta f_j^{(i)}\right) - \left(f_{j-1}^{(i)} + \delta f_{j-1}^{(i)}\right) - \frac{h_j}{2}\left(u_j^{(i)} + \delta u_j^{(i)} + u_{j-1}^{(i)} + \delta u_{j-1}^{(i)}\right) = 0, \quad (30a)$$

$$\left(u_j^{(i)} + \delta u_j^{(i)}\right) - \left(u_{j-1}^{(i)} + \delta u_{j-1}^{(i)}\right) - \frac{h_j}{2}\left(v_j^{(i)} + \delta v_j^{(i)} + v_{j-1}^{(i)} + \delta v_{j-1}^{(i)}\right) = 0, \quad (30b)$$

$$\left(s_j^{(i)} + \delta s_j^{(i)}\right) - \left(s_{j-1}^{(i)} + \delta s_{j-1}^{(i)}\right) - \frac{h_j}{2}\left(t_j^{(i)} + \delta t_j^{(i)} + t_{j-1}^{(i)} + \delta t_{j-1}^{(i)}\right) = 0, \quad (30c)$$

$$\left(v_j^{(i)} + \delta v_j^{(i)}\right) - \left(v_{j-1}^{(i)} + \delta v_{j-1}^{(i)}\right) + \frac{(1+\alpha)\,h_j}{4} \times$$

$$\left[\left(f_j^{(i)} + \delta f_j^{(i)} + f_{j-1}^{(i)} + \delta f_{j-1}^{(i)}\right)\left(v_j^{(i)} + \delta v_j^{(i)} + v_{j-1}^{(i)} + \delta v_{j-1}^{(i)}\right)\right] -$$

$$\frac{h_j}{4}\left(1 + \alpha + \xi\Lambda\right)\left(u_j^{(i)} + \delta u_j^{(i)} + u_{j-1}^{(i)} + \delta u_{j-1}^{(i)}\right)^2 -$$

$$\frac{h_j}{2}\left(M + \frac{1}{DaGr^{1/2}}\right)\left(u_j^{(i)} + \delta u_j^{(i)} + u_{j-1}^{(i)} + \delta u_{j-1}^{(i)}\right) + \frac{\alpha h_j}{2}v_{j-1/2}^{n-1}$$

$$\left(f_j^{(i)} + \delta f_j^{(i)} + f_{j-1}^{(i)} + \delta f_{j-1}^{(i)}\right) - \frac{\alpha h_j}{2}f_{j-1/2}^{n-1}\left(v_j^{(i)} + \delta v_j^{(i)} + v_{j-1}^{(i)} + \delta v_{j-1}^{(i)}\right)$$

$$+\frac{Bh_j}{2}\left[\left(s_j^{(i)} + \delta s_j^{(i)} + s_{j-1}^{(i)} + \delta s_{j-1}^{(i)}\right)\right] = [R_1]_{j-1/2}^{n-1},$$

$$(30d)$$

$$\frac{1}{\Pr}\left[\left(t_j^{(i)} + \delta t_j^{(i)}\right) - \left(t_{j-1}^{(i)} + \delta t_{j-1}^{(i)}\right)\right] + \frac{(1+\alpha)\,h_j}{4} \times$$

$$\left[\left(f_j^{(i)} + \delta f_j^{(i)} + f_{j-1}^{(i)} + \delta f_{j-1}^{(i)}\right)\left(t_j^{(i)} + \delta t_j^{(i)} + t_{j-1}^{(i)} + \delta t_{j-1}^{(i)}\right)\right] + \xi^2 Ec\frac{h_j}{4} \times$$

$$\left[\left(v_j^{(i)} + \delta v_j^{(i)} + v_{j-1}^{(i)} + \delta v_{j-1}^{(i)}\right)^2 + M\left(u_j^{(i)} + \delta u_j^{(i)} + u_{j-1}^{(i)} + \delta u_{j-1}^{(i)}\right)^2\right] +$$

$$+\Omega\frac{h_j}{2}\left(s_j^{(i)} + \delta s_j^{(i)} + s_{j-1}^{(i)} + \delta s_{j-1}^{(i)}\right) - \frac{\alpha h_j}{4} \times$$

$$\left[\left(u_j^{(i)} + \delta u_j^{(i)} + u_{j-1}^{(i)} + \delta u_{j-1}^{(i)}\right)\left(s_j^{(i)} + \delta s_j^{(i)} + s_{j-1}^{(i)} + \delta s_{j-1}^{(i)}\right)\right] +$$

$$+\frac{\alpha h_j}{2}s_{j-1/2}^{n-1}\left(u_j^{(i)} + \delta u_j^{(i)} + u_{j-1}^{(i)} + \delta u_{j-1}^{(i)}\right) - \frac{\alpha h_j}{2}u_{j-1/2}^{n-1} \times$$

$$\left(s_j^{(i)} + \delta s_j^{(i)} + s_{j-1}^{(i)} + \delta s_{j-1}^{(i)}\right) - \frac{\alpha h_j}{2}f_{j-1/2}^{n-1}\left(t_j^{(i)} + \delta t_j^{(i)} + t_{j-1}^{(i)} + \delta t_{j-1}^{(i)}\right) +$$

$$\frac{\alpha h_j}{2}t_{j-1/2}^{n-1}\left(f_j^{(i)} + \delta f_j^{(i)} + f_{j-1}^{(i)} + \delta f_{j-1}^{(i)}\right) = [R_2]_{j-1/2}^{n-1},$$

$$(30e)$$

Next we drop the terms that are quadratic in the following $\left(\delta f_j^{(i)},\ \delta u_j^{(i)},\ \delta v_j^{(i)},\ \delta s_j^{(i)},\ \delta t_j^{(i)} \right)$. We also drop the superscript for simplicity. After some algebraic manipulations, the following linear tridiagonal system of equations is obtained:

$$\delta f_j - \delta f_{j-1} - \frac{h_j}{2}\left(\delta u_j + \delta u_{j-1} \right) = (r_1)_{j-1/2}, \qquad (31a)$$

$$\delta u_j - \delta u_{j-1} - \frac{h_j}{2}\left(\delta v_j + \delta v_{j-1} \right) = (r_2)_{j-1/2}, \qquad (31b)$$

$$\delta s_j - \delta s_{j-1} - \frac{h_j}{2}\left(\delta t_j + \delta t_{j-1} \right) = (r_3)_{j-1/2}, \qquad (31c)$$

$$(a_1)_j \delta v_j + (a_2)_j \delta v_{j-1} + (a_3)_j \delta f_j + (a_4)_j \delta f_{j-1} + (a_5)_j \delta u_j + (a_6)_j \delta u_{j-1}$$
$$+ (a_7)_j \delta s_j + (a_8)_j \delta s_{j-1} = (r_4)_{j-1/2}, \qquad (31d)$$

$$(b_1)_j \delta t_j + (b_2)_j \delta t_{j-1} + (b_3)_j \delta f_j + (b_4)_j \delta f_{j-1} + (b_5)_j \delta u_j + (b_6)_j \delta u_{j-1}$$
$$+ (b_7)_j \delta s_j + (b_8)_j \delta s_{j-1} + (b_9)_j \delta v_j + (b_{10})_j \delta v_{j-1} = (r_5)_{j-1/2}, \qquad (31e)$$

Where

$$(a_1)_j = 1 + h_j \left[\frac{(1+\alpha)}{2} f_{j-1/2} - \frac{\alpha}{2} f_{j-1/2}^{n-1} \right]$$

$$(a_2)_j \;=\; -1 + h_j \left[\frac{(1+\alpha)}{2} f_{j-1/2} - \frac{\alpha}{2} f_{j-1/2}^{n-1} \right],$$

$$(a_3)_j \;=\; h_j \left[\frac{(1+\alpha)}{2} v_{j-1/2} + \frac{\alpha}{2} v_{j-1/2}^{n-1} \right], \qquad (a_4)_j = (a_3)_j,$$

$$(a_5)_j \;=\; h_j \left[-(1+\alpha+\xi\Lambda)\, u_{j-1/2} - \frac{1}{2}\left(M + \frac{1}{DaGr^{1/22}} \right) \right], \qquad (a_6)_j = (a_5)_j,$$

$$(a_7)_j = \frac{B}{2} h_j, \quad (a_8)_j = (a_7)_j \qquad (32)$$

$$(b_1)_j \;=\; \frac{1}{Pr} + h_j \left[\frac{(1+\alpha)}{2} f_{j-1/2} - \frac{\alpha}{2} f_{j-1/2}^{n-1} \right],$$

$$(b_2)_j \;=\; -\frac{1}{Pr} + h_j \left[\frac{(1+\alpha)}{2} f_{j-1/2} - \frac{\alpha}{2} f_{j-1/2}^{n-1} \right],$$

$$(b_3)_j = h_j \left[\frac{(1+\alpha)}{2} t_{j-1/2} + \frac{\alpha}{2} t_{j-1/2}^{n-1} \right],$$

$$(b_4)_j = (b_3)_j, \quad (b_5)_j = h_j \left[M\xi^2 Ecu_{j-1/2} - \frac{\alpha}{2} s_{j-1/2} + \frac{\alpha}{2} s_{j-1/2}^{n-1} \right],$$

$$(b_6)_j = (b_5)_j, \quad (b_7)_j = h_j \left[-\frac{\alpha}{2} u_{j-1/2} - \frac{\alpha}{2} u_{j-1/2}^{n-1} + \frac{\Omega}{2} \right], \qquad (b_8)_j = (b_7)_j,$$

$$(b_9)_j = \left[h_j \xi^2 Ecv_{j-1/2} \right], \qquad (b_{10})_j = (b_9)_j, \tag{33}$$

$$(r_1)_{j-1/2} = f_{j-1} - f_j + h_j u_{j-1/2}, \qquad (r_2)_{j-1/2} = u_{j-1} - u_j + h_j v_{j-1/2},$$

$$(r_3)_{j-1/2} = s_{j-1} - s_j + h_j t_{j-1/2},$$

$$(r_4)_{j-1/2} = (v_{j-1} - v_j) - (1+\alpha) h_j f_{j-1/2} v_{j-1/2} + h_j (1 + \alpha + \xi\Lambda) u_{j-1/2}^2 +$$

$$\left(M + \frac{1}{DaGr^{1/2}} \right) h_j u_{j-1/2} - \alpha h_j v_{j-1/2}^{n-1} f_{j-1/2} + \alpha h_j f_{j-1/2}^{n-1} v_{j-1/2} -$$

$$Bh_j \left[s_{j-1/2} \right] + (R_1)_{j-1/2}^{n-1},$$

$$(r_5)_{j-1/2} = \frac{1}{\mathrm{Pr}} (t_{j-1} - t_j) - (1+\alpha) h_j f_{j-1/2} t_{j-1/2} - \xi^2 h_j Ec \left[(v)^2 + M (u)^2 \right] -$$

$$\Omega h_j s + h_j \alpha u_{j-1/2} s_{j-1/2} - \alpha h_j s_{j-1/2}^{n-1} u_{j-1/2} + \alpha h_j u_{j-1/2}^{n-1} s_{j-1/2} +$$

$$\alpha h_j f_{j-1/2}^{n-1} t_{j-1/2} - \alpha h_j t_{j-1/2}^{n-1} f_{j-1/2} + (R_2)_{j-1/2}^{n-1},$$

$$\tag{34}$$

To complete the system (31), we recall the boundary conditions (25), which can be satisfied exactly with no iteration. Therefore to maintain these correct values in all the iterates, we take:

$$\delta f_0 = 0, \qquad \delta u_0 = 0, \qquad \delta s_0^n = 0, \quad \delta u_J = 0, \qquad \delta s_J = 0 \tag{35}$$

Phase d) Block-tridiagonal Elimination of Linear Keller Algebraic Equations

To linear system (31) can now be solved by the block-elimination method. The linearized difference equations of the system (31) have a *block-tridiagonal structure*. Commonly, the block-tridiagonal structure consists of variables or constants, but here, an interesting feature can be observed that is, for the Keller-box method, it consists of block matrices. Before we can proceed further with the block-elimination method, we will show how to get the elements of the block matrices from the linear system (31). We consider three cases, namely when j = *1, J-1 and J*. When j = 1, the linear systems (31) become:

$$\delta f_1 - \delta f_0 - \frac{h_1}{2}(\delta u_1 + \delta u_0) = (r_1)_{1-1/2}, \tag{36a}$$

$$\delta u_1 - \delta u_0 - \frac{h_j}{2}(\delta v_1 + \delta v_0) = (r_2)_{1-1/2}, \tag{36b}$$

$$\delta s_1 - \delta s_0 - \frac{h_j}{2}(\delta t_1 + \delta t_0) = (r_3)_{1-1/2}, \tag{36c}$$

$$(a_1)_1\delta v_1 + (a_2)_1\delta v_0 + (a_3)_1\delta f_1 + (a_4)_1\delta f_0 + (a_5)_1\delta u_1 + (a_6)_1\delta u_0 \\ +(a_7)_1\delta s_1 + (a_8)_1\delta s_0 = (r_4)_{1-1/2}, \tag{36d}$$

$$(b_1)_1\delta t_1 + (b_2)_1\delta t_0 + (b_3)_1\delta f_1 + (b_4)_1\delta f_0 + (b_5)_1\delta u_1 + (b_6)_1\delta u_0+ \\ (b_7)_1\delta s_1 + (b_8)_1\delta s_0 + (b_9)_1\delta v_1 + (b_{10})_1\delta v_0 = (r_5)_{1-1/2}, \tag{36e}$$

Designating $d_1 = -\frac{1}{2}h_1$, *and* $\delta f_0 = 0$, $\delta u_0 = 0$, $\delta s_0 = 0$, $\delta g_0 = 0$ the corresponding matrix form assumes:

$$\begin{bmatrix} 0 & 0 & 1 & 0 & 0 \\ d_1 & 0 & 0 & d_1 & 0 \\ 0 & d_1 & 0 & 0 & d_1 \\ (a_2)_1 & 0 & (a_3)_1 & (a_1)_1 & 0 \\ (b_{10})_1 & (b_2)_1 & (b_3)_1 & (b_9)_1 & (b_1)_1 \end{bmatrix} \begin{bmatrix} \delta v_0 \\ \delta t_0 \\ \delta f_1 \\ \delta v_1 \\ \delta t_1 \end{bmatrix} +$$

$$\begin{bmatrix} d_1 & 0 & 0 & 0 & 0 \\ 1 & 0 & 0 & 0 & 0 \\ 0 & 1 & 0 & 0 & 0 \\ (a_5)_1 & (a_7)_1 & 0 & 0 & 0 \\ (b_5)_1 & (b_7)_1 & 0 & 0 & 0 \end{bmatrix} \begin{bmatrix} \delta v_1 \\ \delta s_1 \\ \delta f_2 \\ \delta v_2 \\ \delta t_2 \end{bmatrix} = \begin{bmatrix} (r_1)_{1-(1/2)} \\ (r_2)_{1-(1/2)} \\ (r_3)_{1-(1/2)} \\ (r_4)_{1-(1/2)} \\ (r_5)_{1-(1/2)} \end{bmatrix} \tag{37}$$

For $j = 1$, we have $[A_1][\delta_1] + [C_1][\delta_2] = [r_1]$. Similar procedures are followed at the different stations. Effectively the seven linearized finite difference equations have the the matrix-vector form:

$$\boldsymbol{\Theta}\delta_j = \zeta_j \tag{38}$$

where Θ = Keller coefficient matrix of order 5 x 5, δ_j = fifthth order vector for errors (perturbation) quantities and ζ_j= fifthth order vector for Keller residuals. This system is then recast as an *expanded matrix-vector system*, viz:

$$\varsigma_j\delta_j - \omega_j\delta_j = \zeta_j \tag{39}$$

where now ς_j = coefficient matrix of order 5 x 5, ω_j = coefficient matrix of order 5 x 5 and ζ_j= fifthth order vector of errors (iterates) at previous station on grid. Finally the complete linearized system is formulated as a **block matrix system** where each element in the coefficient matrix is a matrix itself. The numerical results are affected by the *number of mesh points* in *both* directions. Accurate results are produced by performing a mesh sensitivity analysis. After some trials in the η-direction a larger number of mesh points are selected whereas in the ξ direction significantly less mesh points are utilized. The edge of the boundary-layer y_∞ was adjusted for different range of parameters. x_{max} is set in the range $[0, \pi]$ for this flow domain.

4   Results and discussion

Selected computations have been conducted to study the influence Forchheimer inertial *Drag parameter* (Λ), *Darcy number (Da)*, *Eckert number (Ec)* and heat source/sink parameter (Ω). In all computations we desire the variation of f' *and* θ versus η (radial coordinate) for the velocity, temperature and species diffusion boundary layers, and also $\frac{1}{2}C_f\sqrt[4]{Gr} = \xi f''(\xi, 0)$ and $\frac{Nu}{\sqrt[4]{Gr}} = -\theta'(\xi, 0)$ versus ξ as a simulation of skin friction function and Nusselt number function with tangential coordinate.

    Figure 4 depicts the **velocity** response$(f')$to various Forchheimer inertial drag parameter (Λ), with radial coordinate η. The Forchheimer drag force term, $-\xi\Lambda f^{/2}$ in the dimensionless momentum conservation equation (5) is quadratic and with an increase in Λ (which is infact related to the geometry of the porous medium) will increase correspondingly. As such the impedance offered by the fibers of the porous medium will increase and this will effectively decelerate the flow in the regime, as testified to by the evident decrease in velocities shown in Figure 4 . The Forchheimer effect serves to super seed the Darcian body force

effect at higher velocities, the latter is dominant for lower velocity regimes and is a linear body force. The former is dominated the lower velocities (the square of a low velocity yields an even lower velocity) but becomes increasingly dominant with increasing momentum in the flow i.e. when inertial effects override the viscous effects (Figure 4).

ξ	$-\theta'(\xi,0)$		
	Merkin	K.A Yih	Present Results
0.0	0.4212	0.4214	0.4214
0.2	0.4204	0.4207	0.4210
0.4	0.4182	0.4184	0.4191
0.6	0.4145	0.4147	0.4153
0.8	0.4093	0.4096	0.4102
1.0	0.4025	0.4030	0.4135
1.2	0.3942	0.3950	0.3966
1.4	0.3843	0.3854	0.3870
1.6	0.3727	0.3740	0.3758
1.8	0.3594	0.3608	0.3617
2.0	0.3443	0.3457	0.3468
2.2	0.3270	0.3283	0.3298
2.4	0.3073	0.3086	0.3103
2.6	0.2847	0.2860	0.2891
2.8	0.2581	0.2595	0.2620
3.0	0.2252	0.2267	0.2312
π	0.1963	0.1962	0.1921

Table 1: Comparision of the values of $-\theta'(\xi,0)$ with M = 0 and Pr = 1

Figure 5 shows that **temperature** θ, is increased continuously through the boundary layer with distance from the cylinder surface, with an increase in Λ, since with flow deceleration, heat will be diffused more effectively via thermal conduction and convection. The boundary layer regime will therefore be warmed with increasing Λ and boundary layer thickness will be correspondingly increased, compared with velocity boundary layer thickness, the latter being reduced.
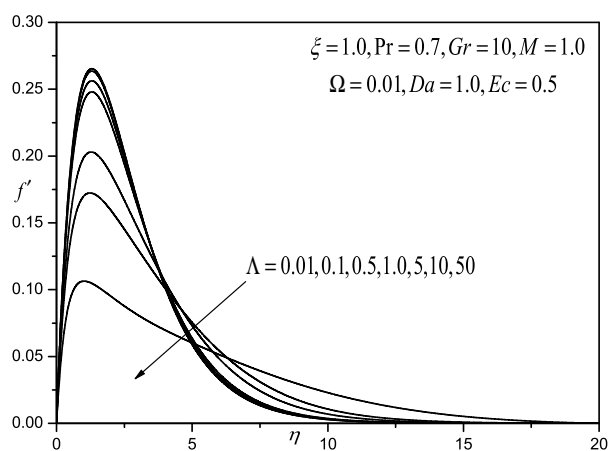
Figure 4: Effect of the Λ on the velocity profiles
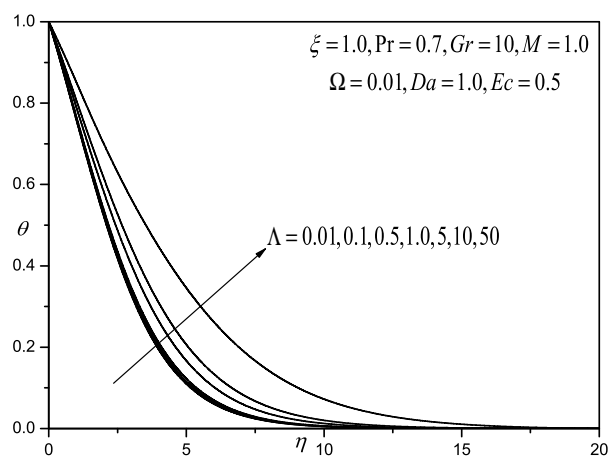
Figure 5: Effect of the Λ on the temperature profiles

Figures 6 show the effect of the **Darcy number** (Da) on dimensionless velocity (f') with transformed radial coordinate (ξ) at a location close to the lower

stagnation point ($\xi = 0.1$). $Da = \frac{K}{a^2}$ for a fixed value of the cylinder radius, a, and free convection parameter, Gr (Grashof number) is directly proportional to permeability, K, of the porous regime. In the momentum conservation equation (5), the Darcian drag term, $-\left(\frac{1}{Da}\right) f'$, is inversely proportional to Da. Increasing Da increases the porous medium permeability and simultaneously decreases the Darcian impedance since progressively less solid fibers are present in the regime. The flow is therefore accelerated for higher Da values causing an increase in the velocity,(f') as shown in figure 6. Maximum effect of rising Darcy number is observed at intermediate distance from the cylinder surface around $\eta \sim 1$. We note that the profiles all correspond to a location some distance from the lower stagnation point on the cylinder at $\xi = 0.5$. Conversely temperature, θ depicted in figure 6 is opposed by increasing Darcy number. The presence of fewer solid fibers in the regime with increasing Da, inhibits the thermal conduction in the medium which reduces distribution of thermal energy. The regime is therefore cooled when more fluid is present and θ values in the thermal boundary layer are decreased. Profiles for both velocity and temperature are smoothly asymptotic decays to the free stream indicating that excellent convergence (and stability) is obtained with the numerical method. Velocity boundary layer thickness will be increased with a rise in Da and thermal boundary layer thickness reduced.
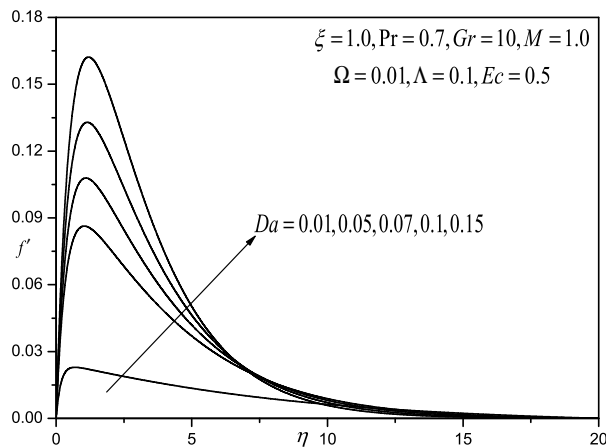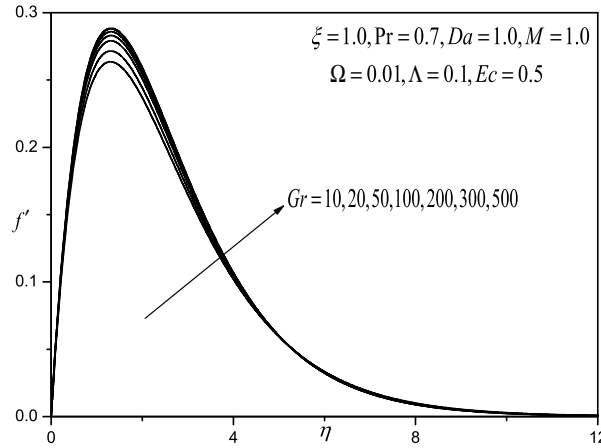

Figure 6: Effect of the *Da* on the velocity profiles

Figure 7: Effect of the Gr on the velocity profiles

The effects of thermal **Grashof number Gr** are shown in **figure 7 to 8** for the velocity, $f\prime$, temperature, θ, distributions. Figure 7 indicates that an increasing Gr from 10 through 20,50, 100,200,300, and 500 strongly boosts velocity. The profiles generally descend smoothly towards zero although the rate of descend is greater corresponding to higher thermal Grashof numbers. Gr defines the ratio of thermal buoyancy force to the viscous hydrodynamic force and as expected does accelerate the flow. Temperature distribution θ versus η is plotted in figure 8 and is seen to decrease with a rise in thermal Grashof number, results which agree with fundamental studies on free convection.

The influence **of heat source** $(\Omega > 0)$ or **heat sink** $(\Omega < 0)$ in the boundary layer on the velocity and temperature fields is presented in **figures 9 and 10**. The presence of heat source in the boundary layer generates energy which cases the temperature of the fluid to increase. This increasing temperature produces an increase in the flow field due to buoyancy effect. On the other hand, the presence of a heat sink in the boundary layer absorbs energy which causes the temperature of the fluid to decrease. This decrease in the fluid temperature causes a reduction in the flow velocity in the boundary layer as a result of the buoyancy effect which couples the flow and thermal problems. These behaviors are depicted in Figures 9 and 10.
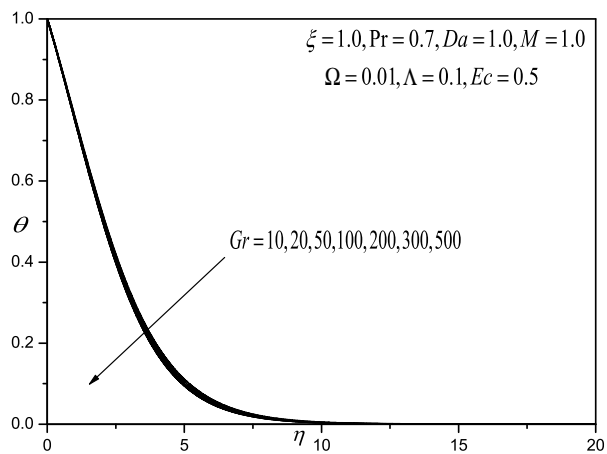
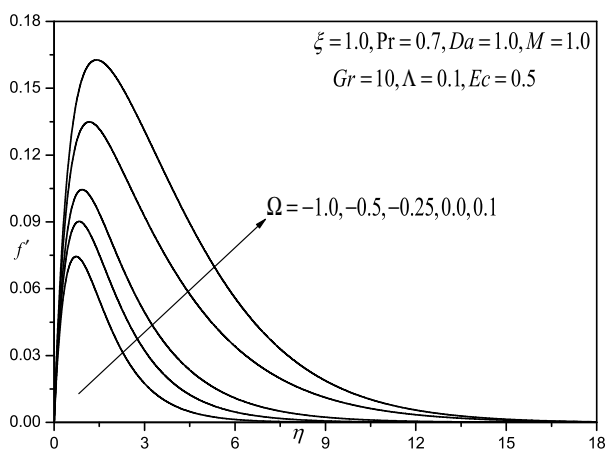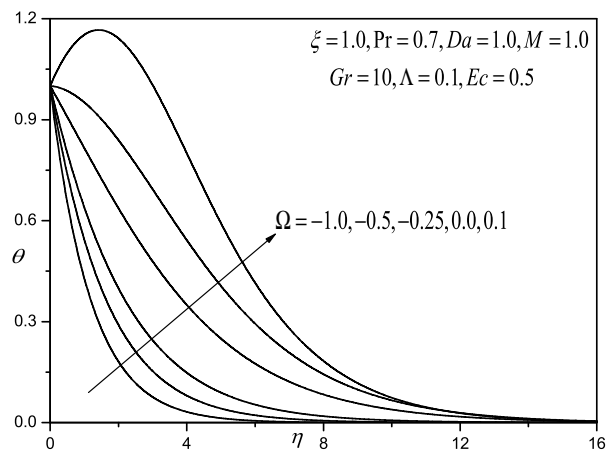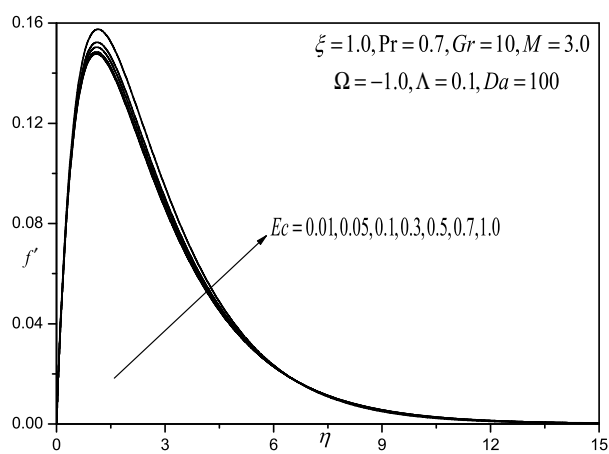Figure 8: Effect of the Gr on the temperature profiles

Figure 9: Effect of the Ω on the velocity profiles.

Figure 10: Effect of the Ω on the temperature profiles.

Figure 11: Effect of the *Ec* on the velocity profiles

The influence of the **Eckert number** i.e. viscous dissipation parameter (Ec) on velocity and temperature profiles is illustrated in **figures 11 and 12**. Ec ex-

presses the relationship between the kinetic energy in the flow and the enthalpy (Schlichting boundary layer theory). It embodies the conversion of kinetic energy into internal energy by work done against the viscous fluid stresses. Although this parameter is often used in high speed compressible flow, for example in rocket aerodynamics at very altitude, it has significance in high temperature incompressible flows, which are encountered in chemical engineering systems, radioactive waste repositories, nuclear engineering systems etc. Positive Eckert number implies cooling of the wall and therefore a transfer of heat to the fluid. Convection is enhanced and we observe in consistency with for example Schlichting and Gersten [47], that the fluid is accelerated i.e. velocity of the fluid is increased as shown in figure 11. Temperatures are boosted as shown in figure 12. Since internal energy is increased.
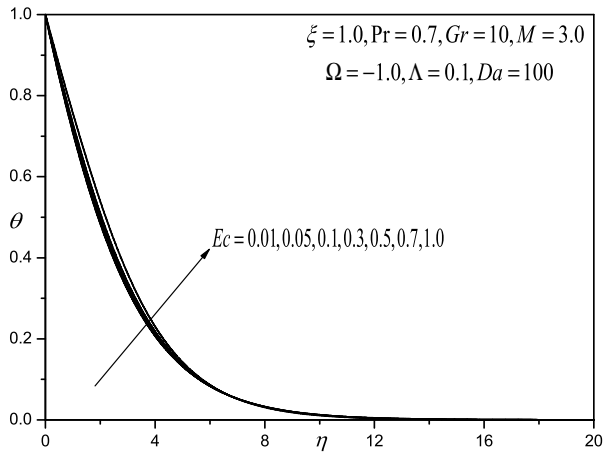

Figure 12: Effect of the Ec on the temperature profiles

Figs.13 to 14 depict the velocity, temperature transverse to the cylinder wall for various stream wise coordinate values, ξ. Velocity is clearly decelerated with increasing migration from the leading edge i.e. larger ξ values (Fig. 13) for some distance into the boundary layer, transverse to the wall ($\eta \sim 30$). However closer to the free stream, this effect is reversed and the flow is accelerated with increasing distance along the cylinder surface. Conversely a very strong increase in temperature (θ), as shown in Figs.14, occurs with increasing ξ values. Also unlike the velocity response which ascends from the surface of the cylinder, peaks

and then decreases further into the boundary layer (Fig.13), the temperature fields decrease continuously across the boundary layer transverse to the wall.
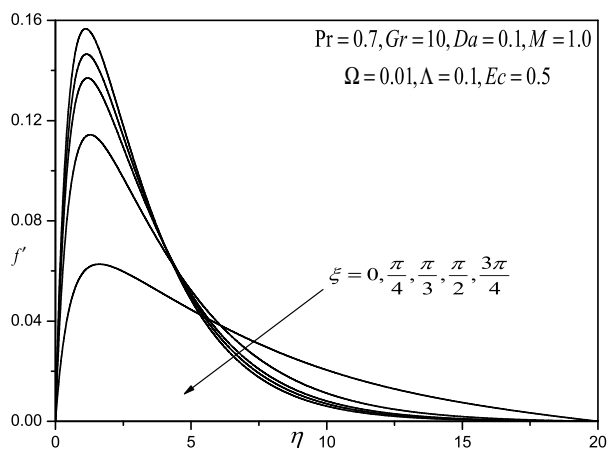

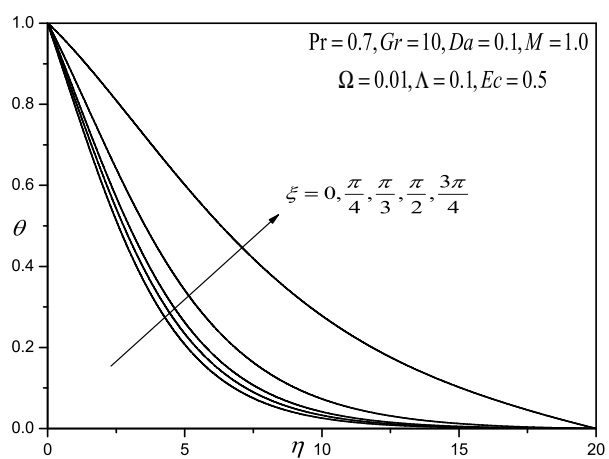Figure 13: Effect of the ξ on the velocity profiles

Figure 14: Effect of the ξ on the temperature profiles

Temperature and concentration are both minimized at the leading edge and maximized with the greatest distances along the cylinder surface from the leading edge.
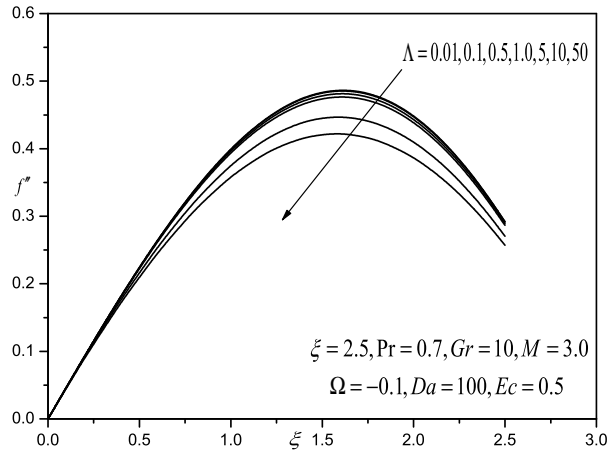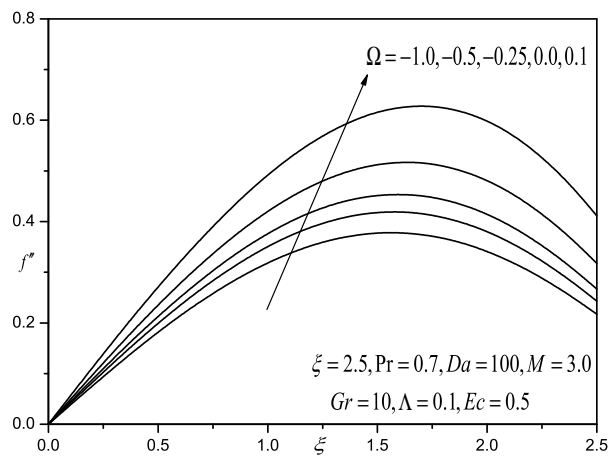

Figure 15: Effect of Λ on the Skin friction coefficient results.

The influence of porosity, Forchheimer parameter on local skin friction at the cylinder surface $(-f^{//})$ with tangential coordinate,ξ, are shown respectively in **figure 15**. Shear stress is progressively enhanced with a rise in ε, but decreased with increasing Λ and M, again confirming that more porous regimes retard the flow less, whereas increasing inertial drag and magnetic field serve to decelerate the flow and reduce shear stresses at the cylinder surface.

Figure 16 to 18 show $f''(\xi,0)\ and\ -\theta'(\xi,0)$ for various values of the Eckert number Ec and heat source/sink parameterΩ. It is seen that the values of $f''(\xi,0)$ increases with increasing the Eckert number Ec and the heat source/sink parameterΩ. On the other hand, enhancing the Eckert number Ec and the heat source/sink parameterΩ reduces the value of $-\theta'(\xi,0)$. This is because that Ec or Ω produces larger dimensionless wall velocity gradient and dimensionless wall temperature.

Figure 16: Effect of Ω on the Skin friction coefficient results
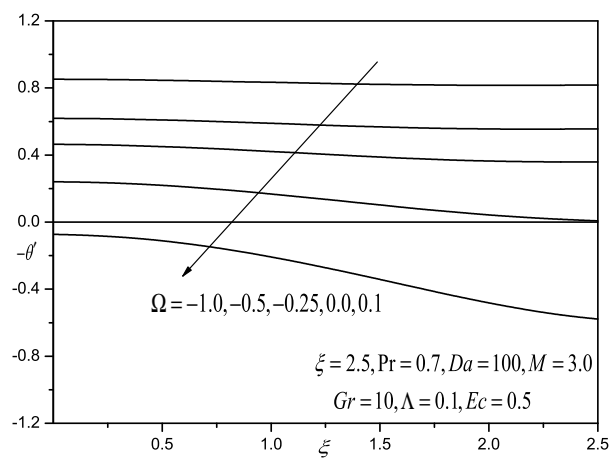
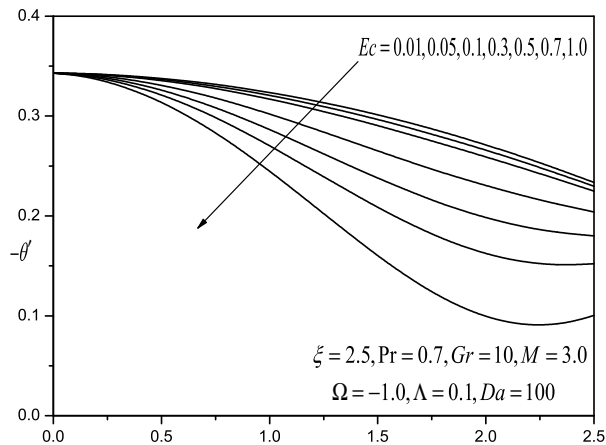Figure 17: Effect of Ω on the local Nusselt number results

Figure 18: Effect of *Ec* on the local Nusselt number results

5 Conclusions

A steady, two-dimensional boundary layer model has been developed for the hydromagnetic viscous flow, heat transfer from a permeable horizontal cylinder, embedded in an isotropic, homogenous, non-Darcian regime, including viscous dissipation and Joule heating effects. A robust, efficient implicit finite difference method introduced by Keller [34] has been implemented to solve the transformed boundary layer equations. Several special cases have been considered. Extensive details of the discretization and matrix algebraic solution procedures have been included. The computations have shown that:

i Increasing magnetic field serves to decelerate the flow and enhance temperature values.

ii Increasing Darcy number accelerates the flow but reduces concentration values.

iii Increasing Forchheimer parameter causes a strong deceleration in the flow.

iv Increasing viscous dissipation parameter acts to accelerate the flow and also enhance temperature values.

v Increasing heat source/sink parameter enhances velocity and also increase temperature values.

vi Increasing Eckert number Ec and heat source/sink parameterΩ reduces the local heat transfer rate (local Nusselt number) at the cylinder surface with the opposite effect sustained for the local skin friction result.

References

[1] Dorfman, K. D. and H. Brenner. 'Generalized Taylor-Aris dispersion in discrete spatially periodic networks: Microfluidic applications', Phys. Rev. E., Vol. 65 (2002), pp. 20-37.

[2] Minkin, L.. 'Thermal diffusion of radon in porous media', *Radiation Protection Dosimetry*, Vol. 106 (2003), pp. 267-272.

[3] Seo,T, H-D. Kim, J-H. Choi and J. H. Chung. 'Mathematical modeling of flow field in ceramic candle filter', *J. Thermal Science, Volume 7* (1998), *pp.* 85-88.

[4] Al-saffar, B. Ozturk and R. Hughes. 'A Comparison of porous and non-porous gas-liquid membrane contactors for gas separation', *IChemE J. Chemical Engineering Research and Design*, Volume 75 (1997), pp. 685-692.

[5] Ledvinkova, B., F. Keller, J. Kosek and U. Nieken. 'Mathematical modeling of the generation of the secondary porous structure in a monolithic adsorbent', *Chemical Engineering J.*, Vol. 140 (2008), pp. 578-585.

[6] Turner, I.W., J.R. Puiggali and W. Jomaa. 'A numerical investigation of combined microwave and convective drying of a hygroscopic porous material: a study based on pine wood', *IChemE J. Chemical Engineering Research and Design*, Vol. 76 (1998), pp 193-209.

[7] Pomés, V., A. Fernandez and D. Houi.. 'Characteristic time determination for transport phenomena during the electrokinetic treatment of a porous medium', *Chemical Engineering J.*, Vol. 87 (2002), pp. 251-260.

[8] Islam, M.R..' Route to chaos in chemically enhanced thermal convection in porous media', *Chemical Engineering Communications*, Vol. 124 (1993), pp. 77-95.

[9] Albusairi, B. and J. T. Hsu. 'Flow through beds of perfusive particles: effective medium model for velocity prediction within the perfusive media', *Chemical Engineering J.*, Vol. 100 (2004), pp. 79-84.

[10] Robert Khachatoorian and Teh Fu Yen.' Numerical modeling of in situ gelation of biopolymers in porous media', *J. Petroleum Science and Engineering,*
Vol. 48 (2005), pp. 161-168.

[11] Arocha, M.A., A. P. Jackman and B. J. McCoy.'Numerical analysis of sorption and diffusion in soil micropores, macropores, and organic matter', *Computers & Chemical Engineering*, Vol. 21 (1996), pp. 489-499.

[12] Zueco, J., Bég, O. A. and Chang, T-B..' Network numerical simulation of two-dimensional nonlinear micropolar hydrodynamics in a Darcian porous medium', *Korean J. Chemical Engineering*, Vol. 26 (2009), pp. 1226-1234.

[13] and Östergren, K.C.E. and C. Trägørdh. 'Modelling and analysis of axial flow through and compression of a non-rigid chromatographic bed', *Chemical Engineering J.*, *Vol. 72 (1999), pp. 153-161.*

[14] Dennis, B.H. and G. S. Dulikravich.' Magnetic field suppression of melt flow in crystal growth', *Int. J. Heat and Fluid Flow, Vol. 23* (2002)*, pp. 269-277.*

[15] Shafieenejad, I., N. Moallemi and A. B. Novinzadeh. 'An analytic approximation of wire coating analysis for third-grade magneto-hydrodynamic flow', *Proc. Inst. Mechanical Engineers, Part C: J. Mechanical Engineering Science*, Vol. 223 (2009), pp. 2273-2280.

[16] Holmes, W.M., R. G. Graham and K. J. Packer (2001).'Diffusion in surface-wetting films in a two-phase saturated porous solid characterised by pulsed magnetic field gradient NMR', *Chemical Engineering J.*, Vol. 83, pp. 33-38.

[17] Garmestani, H., M.S. Al-Haik, K. Dahmen, R. Tannenbaum, D. Li, S.S. Sablin and M.Y. Hussaini.'Polymer-mediated alignment of carbon nanotubes under high magnetic fields', *Advanced Materials*, Vol. 15 (2003), pp. 1918-1921.

[18] Mogi, I., K. Takahashi, S. Awaji, K. Watanabe and M. Motokawa. 'Application of magnetic levitation to processing of diamagnetic materials, *Int. Workshop on Materials Analysis and Processing in Magnetic Field, March 17-19, Tallahassee, USA* (2004).

[19] Bég, O.A., J. Zueco and H.S. Takhar. 'Unsteady magnetohydrodynamic Hartmann–Couette flow and heat transfer in a Darcian channel with Hall current, ionslip, viscous and Joule heating effects: Network numerical solutions', *Communications in Nonlinear Science Numerical Simulation*, Vol. 14 (2009), 1082-1097.

[20] Bég, O.A., J. Zueco, R. Bhargava and H.S. Takhar. 'Magnetohydrodynamic convection flow from a sphere to a non-Darcian porous medium with heat generation or absorption effects: network simulation', *Int. J. Thermal Sciences*, Vol. 48 (2009), pp. 913-921.

[21] Alves, M.A., J.M.P.Q. Delgado, J.R.F. Guedes de Carvalho. 'Mass transfer from cylinders and plane surfaces buried in packed beds in alignment with the flow direction', *Chemical Engineering Science, Vol. 61* (2006)*, pp. 1174-1183.*

[22] Mauguet, M.C., J. Comiti, A. Montillet. 'Liquid–Solid Mass Transfer in Packed Beds of Multisized Cylinders, *IChemE J., Chemical Engineering Research and Design*, Vol. 81 (2003), pp. 1222-1229.

[23] Azzam, G.E.A.,. 'Radiation effects on the MHD mixed free-forced convective flow past a semi-infinite moving vertical plate for high temperature differences', *Phys. Scripta, Vol.* 66 (2002), pp. 71-76.

[24] El-Amin, M.F.. 'Combined effect of viscous dissipation and Joule heating on MHD forced convection over a non-isothermal horizontal cylinder embedded in a fluid saturated porous medium', *J. Magnetism Magnetic Materials*, Vol. 263 (2003), pp. 337-343.

[25] B. Gebhart. 'Effects of viscous dissipation in natural convection' J. Fluid Mech. 14(2), 225-232, (1962).

[26] H.S. Takhar and V.M. Soundalgekar. 'Dissipation effects on MHD free convection flow past a semi-infinite vertical plate' Appl. Sci. Res. 36(3), 163-171, (1980).

[27] E.M. Sparrow and R.D. Cess. 'The effect of a magnetic field on free convection heat transfer' Int. J. Heat Mass Transfer, 3(4), 267-274 (1961).

[28] K.A. Yih. 'Viscous and Joule heating effects on non-Darcy MHD natural convection flow over a permeable sphere in porous media with internal heat generation'. Int. Comm. Heat Mass Transfer, Vol. 27 (2000), No. 4, pp. 591-600.

[29] H.M. Duwairi, Osama Abu-Zeid, Rebhi A. Damesh. 'Viscous and Joule heating effects over an isothermal cone in saturated porous media'. Jordan Journal of Mechanical and Industrial Engineering, Vol. 1 (2007), No. 2, pp. 113-118.

[30] Plumb, O. A. and Huenefeld, T.C.. 'Non-Darcy natural convection form heated surfaces in porous media', *Int. J. Heat Mass Transfer.*, Vol. 24 (1981), pp. 765-768.

[31] Keller, H.B..' A new difference method for parabolic problems', *J. Bramble (Editor), Numerical Methods for Partial Differential Equations* (1970).

[32] Chiam, T.C.. 'The flat plate magnetohydrodynamic boundary layer flow with a step change in the magnetic field', *J. Phys. Soc. Japan.,* Vol. 62 (1993), pp. 2516-2517.

[33] Rees, D.A.S. and I. Pop. 'Boundary layer flow and heat transfer on a continuous moving wavy surface', *Acta Mechanica*, Vol. 112 (1995), pp. 149-158.

[34] Hossain, M.A., S. K. Das and I. Pop.' MHD free convection flow near rotating axisymmetric round-nosed bodies', *Magnetohydrodynamics*, Vol. 32 (1996), pp. 63-67.

[35] Bég, O. A., Takhar, H. S. and Kumari, M.. 'Computational analysis of coupled radiation-convection dissipative nongray gas hydrodynamics in a non-Darcy porous medium using the Keller Box implicit difference scheme', *Int. J. Energy Research*, Vol. 22 (1998), 141-159.

[36] Rees, D. A. S. and M. A. Hossain . 'Combined effect of inertia and a spanwise pressure gradient on free convection from a vertical surface in porous media, *Numerical Heat Transfer, Part A: Applications*, Vol. 36 (1999), pp. 725 – 736.

[37] Bég, O.A., H.S. Takhar, G. Nath and M. Kumari. 'Computational fluid dynamics modeling of buoyancy-induced viscoelastic flow in a porous medium', *Int. J. Applied Mechanics and Engineering*, Vol. 6 (2001), pp. 187-210.

[38] Bég O.A., A. J. Chamkha and H. S. Takhar. 'Radiative free convective non-Newtonian fluid flow past a wedge embedded in a porous medium', *Int. J. Fluid Mechanics Research*, Vol. 31 (2004), pp. 101-115.

[39] Ishak, A., R. Nazar and I. Pop.' Magnetohydrodynamic (MHD) flow and heat transfer due to a stretching cylinder', *Energy Conversion and Management*, Vol. 49 (2008), pp. 3265-3269.

[40] Damseh, R.A., M. S. Tahat and A. C. Benim.' Nonsimilar solutions of magnetohydro-dynamic and thermophoresis particle deposition on mixed convection problem in porous media along a vertical surface with variable wall temperature', *Progress in Computational Fluid Dynamics: An International Journal*, Vol. 9 (2009), pp. 58- 65.

[41] Mishra, S. P. and D. G. Sahoo. 'Magnetohydrodynamic unsteady free convection past a hot vertical plate', *Applied Scientific Research*, Vol. 34 (1978), pp. 1-16

[42] Riley, N., 'Magnetohydrodynamic free convection', *J. Fluid Mechanics*, Vol. 18 (1964), pp. 577-586.

[43] Wilks, G. and R. Hunt. 'Magnetohydrodynamic free convection flow about a semi-infinite plate at whose surface the heat flux is uniform', *Zeitschrift für Angewandte Mathematik und Physik (ZAMP)*, Vol. 35 (1984), pp. 34-49.

[44] H. Schlichting and K. Gersten, Boundary-Layer Theory, MacGraw-Hill, New York, 8th edition, 2000.

Submitted in September 2013.

Računska analiza efekata viskozne disipacije i džulovskog zagrevanja na nedarsijevsko MHD prirodno konvektivno tečenje sa horizontalnog cilindra u poroznoj sredini uz unutrašnje generisanje toplote

Ispitani su uticaji viskozne disipacije, džulovskog zagrevanja i toplotnih izvora (ili ponora) na nedarsijevsko MHD prirodno konvektivno tečenje preko propustljivog horizontalnog cilindra u poroznoj sredini. Jednačine graničnog sloja, parabolične, su normalizovane u nesličan oblik i, potom, rešene numerički pomoću dobro proverene efikasne implicitne i stabilne Keller-ove kutije šeme konačnih razlika. Izvedena je parametarska studija koja ilustruje uticaj Darcy-jevog parametra (Da), Forchheimer-ovog parametra (Λ) , Grashof-ovog broja(Gr), parametra toplotnog izvora/ponora (Ω) kao i parametra viskozne disipacije (Ec) na brzinu fluida, temperaturu, lokalno trenje na zidu kao i Nusselt-ove brojeve. Povećanje Forchheimer-ovog inercijalnog parametra otpora (Λ) vodi ka kašnjenju tečenja ali značajno povećava temperature. Nadjeno je da povećanje parametra viskozne disipacije (Ec) povećava brzine tj. ubrzava tečenje i povećava temperature. Takodje je nadjeno da povećanje parametra toplotnog izvora/ponora (Ω) povećava brzine i izaziva povećanje temperature. Porast Grashof-ovog broja (Gr) vodi ka rastu brzine i opadanju temeperatura. Broj lokalnog trenja na zidu raste sa porastom parametra toplotnog izvora/ponora (Ω), gde lokalni Nusselt-ov broj opada sa porastom parametra toplotnog izvora/ponora (Ω).